

e-MERLIN resolves Betelgeuse at λ 5 cm: hotspots at $5 R_{\star}$

A. M. S. Richards¹, R. J. Davis¹, L. Decin², S. Etoka^{1,3}, G. M. Harper⁴, J. J. Lim^{5,6},
S. T. Garrington¹, M. D. Gray¹, I. McDonald¹, E. O’Gorman⁴, M. Wittkowski⁷

¹JBCA, Dept. Physics and Astronomy, University of Manchester, UK; ²Instituut voor Sterrenkunde, Katholieke Universiteit Leuven, Belgium

³Hamburger Sternwarte, Germany; ⁴School of Physics, Trinity College, Dublin 2, Ireland; ⁵Department of Physics, University of Hong Kong;

⁶Institute of Astronomy and Astrophysics, Academia Sinica, Taipei, Taiwan; ⁷ESO, Garching bei München, Germany.

Accepted MNRAS March 12, 2013

ABSTRACT

Convection, pulsation and magnetic fields have all been suggested as mechanisms for the transport of mass and energy from the optical photosphere of red supergiants, out to the region where the stellar wind is launched. We imaged the red supergiant Betelgeuse at 0.06–0.18 arcsec resolution, using e-MERLIN at 5.5–6.0 GHz, with a sensitivity of $\sim 10 \mu\text{Jy beam}^{-1}$. Most of the radio emission comes from within an ellipse (0.235×0.218) arcsec² ($\sim 5 \times$ the optical radius), with a flux density of 1.62 mJy, giving an average brightness temperature ~ 1250 K. This radio photosphere contains two hotspots of 0.53 and 0.79 mJy beam⁻¹, separated by 90 milli-arcsec, with brightness temperatures 5400 ± 600 K and 3800 ± 500 K. Similar hotspots, at more than double the distance from the photosphere of those seen in any other regime, were detected by the less-sensitive ‘old’ MERLIN in 1992, 1995 and 1996 and many exceed the photospheric temperature of 3600 K. Such brightness temperatures are high enough to emanate from pockets of chromospheric plasma. Other possibilities include local shock heating, the convective dredge-up of hot material or exceptionally cool, low density regions, transparent down to the hottest layer at ~ 40 milliarcsec radius. We also detect an arc 0.2–0.3 arcsec to the SW, brightness temperature ~ 150 K, in a similar direction to extensions seen on both smaller and larger scales in the infra-red and in CO at mm wavelengths. These preliminary results will be followed by further e-MERLIN, VLA and ALMA observations to help resolve the problem of mass elevation from 1 to $10 R_{\star}$ in red supergiants.

Key words: Stars: individual: Betelgeuse – mass-loss – supergiants – Radio continuum: stars

1 INTRODUCTION

Betelgeuse (α Ori), type M2Iab, is the closest red supergiant, with an initial mass of 15–20 M_{\odot} (Dolan et al. 2008). The asymmetric S1 and S2 CO outflows have average velocities and radius limits of 9.8 km s⁻¹, 4 arcsec and 14.3 km s⁻¹, ~ 17 arcsec, respectively (O’Gorman et al. 2012). The mass-loss rate \dot{M} of Betelgeuse is $\sim 10^{-6} M_{\odot} \text{ yr}^{-1}$, estimated by Le Bertre et al. (2012) from a 0.24-pc HI shell. Its proper motion is towards the NE and a bow shock was identified in the infra-red (IR) (Noriega-Crespo et al. 1997) and HI and mapped using *Herschel* (Decin et al. 2012), which shows arcs 6–7 arcmin NE of the star. We adopt the 2.2 μm photospheric radius ~ 22.5 milli-arcsec (mas) (Dyck et al. 1996; Perrin et al. 2004) as R_{\star} , at a distance of ~ 197 pc (Harper et al. 2008).

Mass loss from cool, evolved stars (e.g. VX Sgr) which form copious dust at ~ 5 – $10 R_{\star}$, is thought to be initiated by pulsations, followed by radiation pressure on dust accelerating the wind to escape velocity (Bowen 1988). However, the requirements for this mechanism do not seem to be present in early M-type stars like Betelgeuse. It shows weaker optical variability (Percy et al. 1996) than the RSG which form more dust. Verhoelst et al. (2006) found signs of metal oxide nucleation at $\sim 1.5 R_{\star}$ but silicates have only

been found at radii ≥ 500 mas (e.g. Tatebe et al. 2007; Skinner et al. 1997). Dupree et al. (1987) measured periodicities in optical and ultraviolet fluxes probably tracing pulsational shock waves which could help to initiate mass outflow. Other potential mass-loss mechanisms include localised events related to convection (e.g. as modelled by Chiavassa et al. 2010). Aurière et al. (2010) measured a longitudinal magnetic field of 0.5–1.5 G, leading to models for magnetic promotion of mass loss (Thirumalai & Heyl 2012). See the Proceedings of the Betelgeuse 2012 workshop, eds. Kervella et al., in prep., for more comprehensive reviews of mass loss studies.

VLA observations by Lim et al. (1998) at 43, 22, 15, 8 and 5 GHz showed the measured radius increasing from 2–7 R_{\star} . The opacity increases with decreasing frequency, so lower frequency images sample layers at larger radii, found to be cooler. Over this range of R_{\star} , the radio brightness temperature T_b falls from ~ 3540 – 1370 K and the photosphere becomes cool enough for dust to begin to form. However, Uitenbroek et al. (1998) detected UV continuum and lines formed at ≥ 5000 K, at radii of up to 2.8 and 6 R_{\star} , respectively. Absorption lines reveal a rotation speed of 5 km s⁻¹ and they suggest that a bright spot in the SW defines the orientation of the rotational axis, at a position angle of 55°, giving a

deprojected rotation period of 25 yr at 14° yr^{-1} . The chromospheric tracer MgII shows an expansion velocity of 10 km s^{-1} , detected out to almost $9 R_\star$ (Gilliland & Dupree 1996). Asymmetric absorption lines such as H α (Weymann 1962; Bagnulo et al. 2003) suggest outflow of chromospheric material at $5\text{--}7 \text{ km s}^{-1}$.

Lim et al. (1998) deduced that the chromospheric gas must be at least a thousand times less abundant than the material dominating radio emission, ruling out global heating as a mass-loss mechanism, leaving convection as a plausible alternative. Harper & Brown (2006) studied multi-epoch spatially resolved HST spectra and, by measuring the electron density and comparing it to 22-GHz observations, confirmed the small filling factor. Chromospheric emission lines suggested rotation about an axis at a position angle of 65° at a velocity not exceeding $\sim 5 \text{ km s}^{-1}$, suggesting that chromospheric material is not in solid-body rotation at $R > 75 \text{ mas}$.

We observed Betelgeuse using e-MERLIN at 5.5–6.0 GHz ($\lambda \approx 5.2 \text{ cm}$), providing ~ 4 resolution elements across the stellar diameter. These are the first well-resolved images at cm wavelengths, investigating whether the irregularities seen at 43 GHz ($\lambda 7 \text{ mm}$) persist at larger radii. We describe the observations in Section 2 and results in Section 3, discussing these in Section 4. We suggest future work in Section 5 and conclude with a summary in Section 6.

2 OBSERVATIONS AND DATA REDUCTION

2.1 2012 e-MERLIN observations

Betelgeuse was observed in the first semester of e-MERLIN open time on 13–15 July 2012, with a bandwidth of 0.512 GHz centred on 5.75 GHz. Seven antennas were used including the 75-m Lovell telescope providing baselines from 11–217 km (90–3910 k λ). The data were processed in dual polarization, using $4 \times 128 \text{ MHz}$ spectral windows, each divided into 64 2-MHz channels. The point-like QSO 0551+0829, separation 1.5° , was used as the phase reference on a cycle of 7:3 min. OQ208 was used as the bandpass and flux density calibrator. Calibration is summarized in Appendix A. The flux scale is accurate to $\sim 10\%$ and the astrometric uncertainty arising from phase referencing is 16 mas. The calibrated and edited Betelgeuse data comprised 4–8 hr per antenna, spread over 10.5 hr, with an average bandwidth of 400 MHz.

We made two maps after self-calibration, using different weighting schemes (see Appendix A). We maximised sensitivity using a 3500-k λ taper and a circular 180-mas (FWHM) restoring beam. This produced a noise $\sigma_{\text{rms}} = 0.027 \text{ mJy beam}^{-1}$. We maximised resolution by applying partial uniform weighting (ROBUST 0.75) and using a restoring beam of $(80 \times 60) \text{ mas}^2$ at position angle (PA) 143° (close to the natural beam shape), giving $\sigma_{\text{rms}} = 0.009 \text{ mJy beam}^{-1}$. Despite the lower noise per beam, the minimum brightness temperature sensitivity limit is 225% higher with this weighting. In order to ensure artifacts were not introduced, we made images with completely natural weighting (used for astrometry) and with the above weightings, prior to self-calibration. The high-resolution dirty map has σ_{rms} of $0.03 \text{ mJy beam}^{-1}$, with peaks of 0.81 and $0.63 \text{ mJy beam}^{-1}$, similar to the features described in Section 3.3.

2.2 Archival data

We retrieved MERLIN Betelgeuse data observed at 4.994 GHz on 1995-06-24 and 1996-11-03 (Morris 2001) using 16 MHz bandwidth, and VLA data observed at 4.885 GHz on 1996-10-21 using 100 MHz bandwidth. These data sets were reduced using stan-

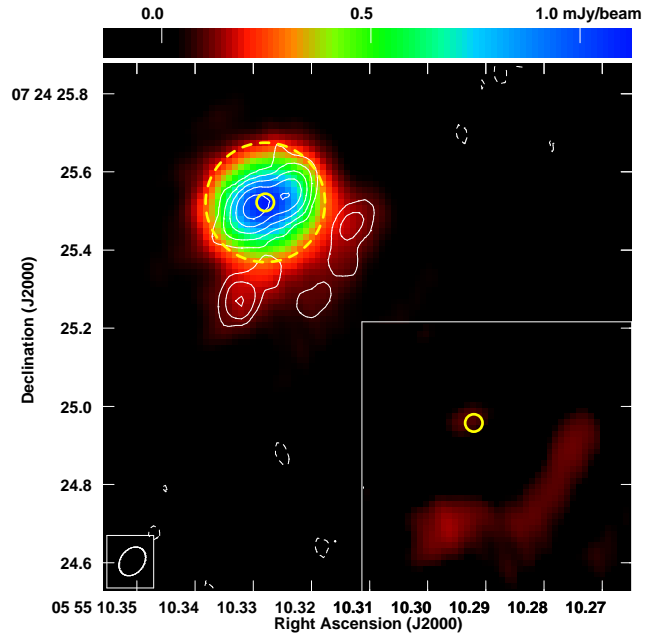


Figure 1. The main panel shows the 2012 e-MERLIN colour image of Betelgeuse optimised for sensitivity to extended structure, using a beam size of 180 mas, $\sigma_{\text{rms}} = 0.027 \text{ mJy beam}^{-1}$. The contours of the image optimised for resolution are overlaid, with the beam size at lower left, the noise $\sigma_{\text{rms}} = 0.009 \text{ mJy beam}^{-1}$, and contour levels at $(-1, 1, 2, 4, 8, 16) \times 0.027 \text{ mJy beam}^{-1}$. The small, solid yellow circle is the size of the 45-mas diameter photosphere, centred on the low-resolution peak, and the large, dashed circle shows the 310-mas, 5-GHz disc (Lim et al. 1998). The insert shows the SW arc after subtracting the central star, on the same scale.

dard techniques (Diamond et al. 2003, Greisen 1994). The MERLIN data were imaged with natural weighting (beam size $(85 \times 55) \text{ mas}^2$) and no cleaning, giving σ_{rms} of 0.15 and $0.12 \text{ mJy beam}^{-1}$ in 1995 and 1996, respectively. The 1996 MERLIN and VLA data were combined to give a resolution of 200 mas and σ_{rms} of $0.058 \text{ mJy beam}^{-1}$; the VLA-only image had 400-mas resolution.

3 RESULTS

3.1 Extended structure seen in 2012

Figure 1 shows the colour image made with optimum sensitivity to extended structure, using a 180-mas restoring beam. The peak is $1.116 \text{ mJy beam}^{-1}$. The $3\sigma_{\text{rms}}$ boundary ($0.081 \text{ mJy beam}^{-1}$ at this resolution), represented by the limit of red shading, has a quite irregular outline, with a maximum extent of 550 mas approximately N–S. The shortest, radial separation between the peak and the $3\sigma_{\text{rms}}$ limit is about 190 mas, to the NNE. We fitted a 2D elliptical Gaussian component to this image, yielding a total flux density $1.619 \pm 0.057 \text{ mJy}$ at position $05:55:10.3274 +07:24:25.514$, with a noise-based uncertainty of 4 mas. The component had major and minor axes ($\theta_{\text{maj}}, \theta_{\text{min}}$) of $(235 \times 218) \text{ mas}^2$, uncertainty $\sigma_\theta = 6 \text{ mas}$, PA $115 \pm 9^\circ$ (significantly different from the beam PA of 143°).

The brightness temperature of a component of flux density S , area A , is given in Kelvin by

$$T_b = 15400 \left(\frac{S}{\text{mJy}} \right) \left(\frac{\lambda}{\text{m}} \right)^2 \left(\frac{A}{\text{arcsec}^2} \right)^{-1}. \quad (1)$$

We observed at wavelength $\lambda = 0.052 \text{ m}$. The area of a Gaussian

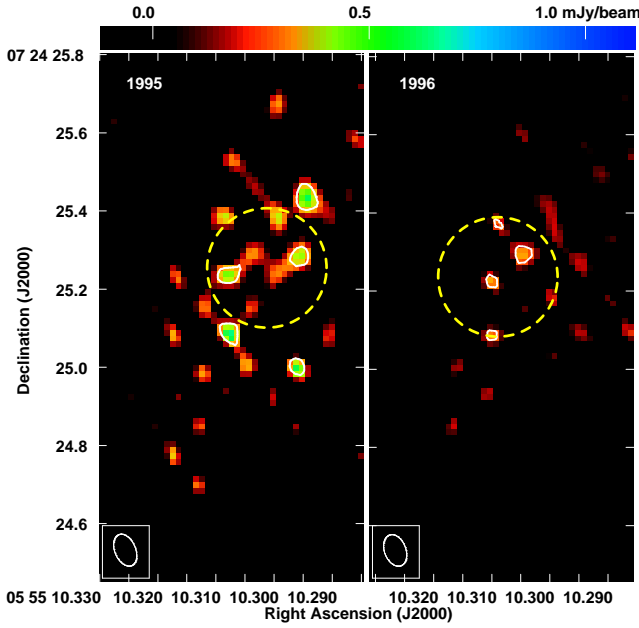


Figure 2. MERLIN images of Betelgeuse observed at 4.994 GHz in 1995 and 1996, contours at 0.60 and 0.48 mJy beam⁻¹ ($4\sigma_{\text{rms}}$), respectively, using the same angular scale as Fig. 1. The beam size is (85×55) mas². The large, dashed circle shows the 310-mas, 5-GHz disc (Lim et al. 1998).

component is given by $A = \pi(\theta_{\text{maj}}\theta_{\text{min}})/(4 \ln 2)$. The main component thus has $T_b = 1170 \pm 135$ K. There is a point-like residual of 0.082 mJy beam⁻¹ (only just over $3\sigma_{\text{rms}}$) at the position of the peak, contributing another ~ 100 K, giving $T_b = 1250 \pm 150$ K within a radius of $\sim 5 R_*$. This is close to the temperature and the size (dashed circle in Figs. 1 to 3) measured by Lim et al. (1998) by fitting a uniform disc to the 5-GHz VLA visibilities, showing the stability of these atmospheric conditions over 16 yr.

The residuals after subtracting the central component are shown in the insert of Fig. 1. There is a substantial arc in the SW quadrant, with a maximum extent above $3\sigma_{\text{rms}}$ of 510 mas with a total flux density 0.088 ± 0.019 mJy in 0.0249 arcsec². It has an irregular outline but is approximately 100 mas wide, at a radius between ~ 175 – 275 mas from the central peak. The SW arc has an average $T_b = 150 \pm 40$ K.

3.2 Position and flux density

Our first map of Betelgeuse (phase-reference solutions only) had a peak of 0.78 ± 0.063 mJy beam⁻¹ at 05:55:10.3267 +07:24:25.525. The noise-based position uncertainty is 9 mas and the total astrometric uncertainty (mostly due to the 1.5° separation from the phase reference source) is 20 mas. Harper et al. (2008) used *Hipparcos* and multi-epoch VLA data to solve for position, proper motion and parallax, up to epoch 2004.829. The preferred solution (their number 5) predicts a position of 05:55:10.3250 +07:24:25.536, uncertainty (5, 6) mas at our epoch, 2012.536. This is (25, 10) mas from our position, close to the combined uncertainties.

The total flux density of 1.62–1.71 mJy (depending on whether the SW arc is enclosed) measured at 5.75 GHz, is equivalent to $(1.3\text{--}1.4) \pm 0.2$ mJy at 4.85 GHz, using a spectral index of 1.32 (Newell & Hjellming 1982), allowing for the uncertainty in this extrapolation. Observations at 4–8–4.9 GHz showed a decline from 2 to 1.2 mJy during 1981 to 2002, fluctuating within the range

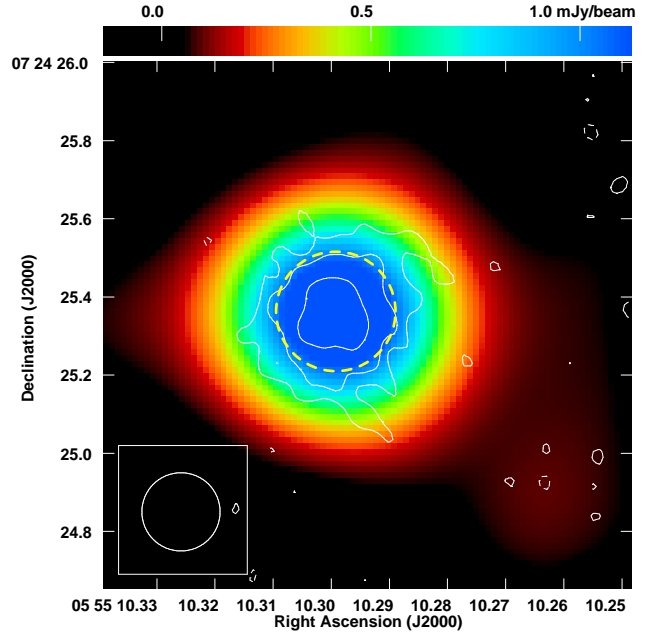


Figure 3. 1996 combined MERLIN+VLA image of Betelgeuse (contours at $(-1, 1, 2, 4) \times 0.17$ mJy beam⁻¹), beam size 200 mas, overlaid on the VLA-only image observed at 4.9 GHz, beam size 400 mas. The angular scale is the same as Fig. 1. The large, dashed circle shows the 310-mas, 5-GHz disc (Lim et al. 1998).

0.9–1.3 mJy up to 2004 (Newell & Hjellming 1982, Skinner et al. 1997, Lim et al. 1998; Harper & Brown private communication).

3.3 Hotspots seen in 2012

The contours in Fig. 1 show the image optimised for resolution, using a (80×60) mas² restoring beam. Two individually-unresolved peaks appear, with flux densities and positions of 0.706 mJy beam⁻¹ at 05:55:10.3299 +07:24:25.510 and 0.489 mJy beam⁻¹ at 05:55:10.3241 +07:24:25.541, respectively (measured by fitting two Gaussian components simultaneously). $\sigma_{\text{rms}} = 0.0095$ mJy beam⁻¹ and the noise-based position uncertainties are 1 mas for the brighter peak and 2 mas for the fainter one. The hotspots are separated by 90 ± 10 mas, at a PA of $(110 \pm 10)^\circ$. This is similar to the orientation of the major axis of the Gaussian component fitted to the emission imaged at 180-mas resolution (Section 3.1) and significantly different from the beam PA. The peaks are separated by $> 20\sigma$ in both position and flux density. Their brightness temperatures are $T_b = 5400 \pm 600$ K and $T_b = 3800 \pm 500$ K, uncertainties dominated by the overall flux scale uncertainty.

3.4 1995 – 1996 MERLIN and VLA results

Figure 2 shows that, at the lower sensitivity of the ‘old’ MERLIN archive data, just a few hotspots were detected at the position of Betelgeuse. In 1995, 5 spots brighter than 0.60 mJy beam⁻¹ ($4\sigma_{\text{rms}}$) were detected, the brightest at 0.78 mJy beam⁻¹. In 1996, 4 spots brighter than 0.48 mJy beam⁻¹ ($4\sigma_{\text{rms}}$) were detected, the brightest at 0.56 mJy beam⁻¹. The formal position uncertainties are ~ 40 mas but may be higher due to calibration errors. The shortest baseline (11 km) allows scales as large as 0.5 arcsec to be imaged, and the sensitivity of the 1995 and 1996 images corresponds approximately

to the highest contour in Fig. 1, so the non-detection of most of the stellar disc was due to lack of sensitivity rather than missing spacings. The peak brightness temperatures (at $\lambda = 0.061$ m) were $T_b = 8000 \pm 2000$ K in 1995 and $T_b = 6000 \pm 2000$ K in 1996. The uncertainties are too high to draw any firm conclusions from the distribution of the spots.

The contours in Fig. 3 show the 1996 combined MERLIN+VLA image, containing 1.69 ± 0.17 mJy in a Gaussian component with $(\theta_{\text{maj}}, \theta_{\text{min}})$ of (289×256) mas², σ_θ 17 mas, PA $(150 \pm 30)^\circ$. This gives $T_b = 1200 \pm 200$ K. The colour image shows the 1996 VLA-only data, which were part of a multi-frequency dataset analysed by Lim et al. (1998) and Harper & Brown (2003), who measured a flux density of 1.77 ± 0.09 mJy. The VLA image contains a faint feature 0.6 arcsec due SW of the peak (over twice the distance to the e-MERLIN arc), at 0.095 mJy beam⁻¹, just over $3\sigma_{\text{rms}}$.

4 DISCUSSION

4.1 SW Arc

The SW arc is at a radius of ~ 250 mas, where, according to the semi-empirical model of Harper et al. (2001), the electron temperature T_e is ~ 900 K and the hydrogen number density $n_H \sim 5 \times 10^{13}$ m⁻³. This gives an optical depth ~ 0.18 for the observed $T_b \sim 150$ K. Assuming that the arc is as deep as it is wide, we approximate the region producing most of the emission by a spheroid with semi-major axes of 10, 10 and 25 au, giving a hydrogen mass of $\sim 1.8 \times 10^{-6} M_\odot$, suggesting that one such clump could be formed every couple of years.

The arc is about 100 mas outside the 6-GHz photospheric radius, in a similar direction to the CN plume seen by Kervella et al. (2009) at $\lesssim 6 R_\star$ and the faint SW extension at ~ 0.6 arcsec seen at 5 GHz in 1996. A clump of CO emission was seen in 2007 by O’Gorman et al. (2012) just outside the S1 shell, 5 arcsec SW of the centre, suggesting a wind travel time of ~ 500 yr at 9 km s⁻¹. These observations suggest repeated or continuous ejections, rather than proper motion of a single clump. This is also aligned with the SW pole of the rotational axis identified by Uitenbroek et al. (1998). The direction could be coincidence, since observations at $7.76\text{--}19.5$ μm in Nov 2010 (Kervella et al. 2011) show clumps outside the photosphere at $0.8\text{--}1.7$ arcsec around more than a semi-circle, between NE and S. A comparison with the direction of the bow shock seen $6\text{--}7$ arcmin to the NE (Decin et al. 2012) is tempting, but structures on sub-arcmin scales are deep within the astropause and should share the proper motion of the star.

4.2 Hotspots

The $5\text{--}6$ GHz hotspots, measured at $55\text{--}85$ mas resolution, have T_b formally above the peak photospheric temperature of 3600 K (Dyck et al. 1996), similar to the chromospheric temperature, which could reach 8000 K (Harper & Brown 2006). We used conservative uncertainties, dominated by the maximum uncertainty in the flux scale, although the good agreement with VLA results for the whole-disc flux density suggests our uncertainties may be overestimated. One or more hotspots are significantly hotter than the photosphere in 2012, 1996 and 1995 and also in the 1992 MERLIN observations imaged at full resolution (Morris 2001). Note that, at the sensitivity of old MERLIN, no emission at all at $T_b \lesssim 4500\text{--}6000$ K (depending on epoch) would have been detected.

The radio photosphere major axis is at $110\text{--}115^\circ$ in the fully-calibrated 2012 data, compared with $(67 \pm 7)^\circ$ at 43-GHz in 1998 (Lim et al. 1998). The orientation of the optical disc and hot spots also varies; the ~ 20 mas axis joining the two hotspots seen by Haubois et al. (2009) is approximately NE–SW. Four sets of IR observations over 24 months by Tuthill et al. (1997) showed $2\text{--}3$ hotspots at a variety of position angles within the inner ~ 100 mas.

Harper & Linsky (2001) showed that increasing the local T_e $2\text{--}3$ -fold enhances radio emission much more effectively than increasing the gas density by the same factor. There are several possible origins for hotspots:

- (i) Levitation of gas from the inner photosphere, e.g. by convection, although such gas would cool radiatively and by expansion.
- (ii) Exceptionally cool, small patches in the outer layers, transparent enough to expose hotter, inner layers. The separation of the 2012 hotspots is 90 ± 10 mas, similar to the 80 -mas diameter of the hottest layer (where the greatest chromospheric contribution to emission is greatest, Harper & Brown 2006, using 197 pc distance).
- (iii) Shock heating due to pulsations and/or convection;
- (iv) Chromospheric patches at $\sim 5 R_\star$ heated by acoustic and/or magnetic processes.

Options (iii) and/or (iv) seem most likely to produce radio hot spots $\gtrsim 4000$ K. Ireland et al. (2011) modelled pulsation in Miras out to $5 R_\star$, finding average effective temperatures $\lesssim 3800$ K. Large-scale up- and down-flows are seen in chromospheric lines, including directional reversals at up to $\sim 3 R_\star$, measured by Lobel & Dupree (2001). Ohnaka et al. (2011) measured up- and down-draughts of CO, within $\sim 2.5 R_\star$, at $\lesssim 30$ km s⁻¹, with different velocities occurring simultaneously on different sides of the star. Such speeds are sufficient to supply shock heating even if it is not clear how convection could operate at $\gg 2.5 R_\star$. Wittkowski et al. (2011) made spectro-interferometric observations, around 2 μm , of continuum and clumpy molecular layers around AGB stars, which suggested pulsation- and shock-induced chaotic motion, not requiring convection. Most radio emission is non-chromospheric (Section 1), but the hotspots have $T_b \lesssim 8000$ K, in the chromospheric range. Harper & Brown (2006) suggest that chromospheric gas is confined within magnetic fields; dissipation of magnetic energy may continue to heat the gas even at high elevations.

5 FURTHER HIGH-RESOLUTION STUDIES

We have shown that both cool, extended radio-continuum emission and hot starspots on Betelgeuse can be resolved at $5.5\text{--}6$ GHz. Multi-epoch, multi-frequency follow-up is needed to establish the emission mechanisms and role in mass loss. In full operations, e-MERLIN will reach 0.002 mJy beam⁻¹ in two full tracks at $5\text{--}7$ GHz. Proper motions of 5 km s⁻¹ could be measured in 4 months for a spot 0.3 mJy brighter than its surroundings, revealing whether the hotspots rotate as predicted for the chromosphere. The variability timescale will constrain the underlying mechanism. Modelling by Harper & Linsky (2001) shows that CII recombination to CI takes ~ 2 months at $n_H \sim 4 \times 10^{14}$ m⁻³, around $5 R_\star$, or longer at higher radius, and chemical changes have similar timescales, but mechanisms involving bulk up-/down-draughts alone would take about a year to produce comparable changes.

Matching resolution at 50 mas can be achieved by the EVN, e-MERLIN and the Karl G. Jansky VLA (alone or in combination as required) at $1.4\text{--}50$ GHz, and eventually by ALMA at higher frequencies. Finer resolution (≤ 20 mas) is possible at 22 GHz and

some higher frequencies, suited to the smaller observed size of the radio photosphere. This will allow us to resolve the spectral indices of the extended emission and the hotspots and test models for localised heating (Harper et al. (2001) and references therein). For example, a decrease of T_e with decreasing frequency above a hot spot would suggest a chromospheric, rather than convective origin.

The average radius (Lim et al. 1998) is approximately related to the observing frequency in GHz by $R(\nu) \sim 55\nu^{-0.5}$ au. At a speed of 10 km s^{-1} (within the range shown by chromospheric lines, Gilliland & Dupree 1996), it would take 0.5 yr for a disturbance to propagate 1 au from surfaces optically thick at 25 GHz to 21 GHz, and 1 yr from the 6 GHz to the 5 GHz surface. Monitoring at decreasing frequencies, i.e. increasing radii, at suitable intervals, will track the evolution of disturbances. This will show whether we are witnessing phenomena propagating outwards smoothly, or localized changes behaving differently, helping to distinguish between convection and pulsation. We will resolve CO, other molecules and dust using ALMA, thus measuring the composition and mass of the wind. Clumps will be resolved on scales of a few au, within a few tens au from the star, where chemistry is still active, overlapping with the scales resolved in the MIR (Kervella et al. 2011).

6 SUMMARY

e-MERLIN has produced the highest-resolution images of Betelgeuse at cm wavelengths, in July 2012. The 5.75 GHz photosphere is fitted by a 2-D Gaussian component, axes $(0.235 \times 0.218) \text{ arcsec}^2$ ($\sim 5R_*$), flux density 1.62 mJy, with an average brightness temperature $\sim 1250 \text{ K}$. Extrapolating to 4.9 GHz shows that the flux density decline since 1981 may have levelled off; the large-scale size and brightness is consistent with the results from Lim et al. (1998). The peak position is close to the position predicted from the proper motion analysis by Harper et al. (2008). An arc is seen $0.2\text{--}0.3 \text{ arcsec}$ to the SW, brightness temperature $\sim 150 \text{ K}$, hydrogen mass $\sim 1.8 \times 10^{-6} M_\odot$. It is in the same direction as IR plumes seen on smaller and larger scales (Kervella et al. 2009; Kervella et al. 2011), a faint 4.9-GHz feature at 0.6 arcsec seen in 1996 and CO emission imaged by O’Gorman et al. (2012). This suggests persistent ejection in this direction for several centuries.

e-MERLIN resolved two distinct peaks, 90 mas apart within the larger stellar disc, with brightness temperatures 4000–6000 K. These are likely to be hot spots at $\sim 5 R_*$, although it is possible that cooler, low-opacity inhomogeneities in higher layers reveal the hottest chromospheric layers. Similar, isolated peaks were also detected by MERLIN observations in 1992, 1995 and 1996. Such high-sensitivity, high-resolution radio continuum observations can resolve emission simultaneously from material at chromospheric and photospheric temperatures, and have the potential to track proper motions. Future multi-frequency imaging with e-MERLIN, the VLA and ALMA will investigate whether the signatures of chromospheric emission, convection or pulsation shocks are seen in the radio photosphere from $2\text{--}10 R_*$, helping to elucidate the mechanisms which eject material from the star into its envelope.

7 ACKNOWLEDGMENTS

We warmly thank M. K. Argo, R. Beswick, and the rest of the e-MERLIN team for guidance in reducing these data. e-MERLIN is the UK radio interferometer array, operated by the University of Manchester on behalf of STFC. We are very grateful to the referee

for insightful comments which improved the accuracy of this paper. We acknowledge the use of MERLIN and VLA archival data.

REFERENCES

- Aurière M., Donati J.-F., Konstantinova-Antova R., Perrin G., Petit P., Roudier T., 2010, *A&A*, 516, L2
 Bagnulo, S. et al. 2003, *The Messenger*, 114, 10
 Bowen G. H., 1988, *ApJ*, 329, 299
 Chiavassa, A. et al. 2010, *A&A*, 511, A51
 Decin, L., et al. 2012, *A&A*, 548, 113
 Diamond, P. J. et al. 2003, *MERLIN User Guide*
 Dolan M., Mathews G. J., Dearborn D., 2008, in *Nuclei in the Cosmos (NIC X) Evolutionary Tracks for Betelgeuse*
 Dupree A. K., Baliunas S. L., Hartmann L., Nassiopoulos G. E., Guinan E. F., Sonneborn G., 1987, *ApJL*, 317, L85
 Dyck H. M., van Belle G. T., Ridgway S. T., 1996, *AJ*, 111, 1705
 Gilliland R. L., Dupree A. K., 1996, *ApJ*, 463, L29
 Greisen E., ed. 1994, *AIPS Cookbook*. NRAO Charlottesville
 Harper G. M., Brown A., 2003, in Piskunov N., Weiss W. W., Gray D. F., eds, *Modelling of Stellar Atmospheres* p. 11
 Harper G. M., Brown A., 2006, *ApJ*, 646, 1179
 Harper G. M., Brown A., Guinan E. F., 2008, *AJ*, 135, 1430
 Harper G. M., Brown A., Lim J., 2001, *ApJ*, 551, 1073
 Harper G. M., Linsky J. L., 2001, in Garcia Lopez R. J., Rebolo R., Zapaterio Osorio M. R., eds, *11th Cambridge Workshop on Cool Stars, Stellar Systems and the Sun Vol. 223*. p. 1603
 Haubois, X. et al. 2009, *A&A*, 508, 923
 Ireland M. J., Scholz M., Wood P. R., 2011, *MNRAS*, 418, 114
 Kervella P., Perrin G., Chiavassa A., Ridgway S. T., Cami J., Haubois X., Verhoelst T., 2011, *A&A*, 531, A117
 Kervella P., Verhoelst T., Ridgway S. T., Perrin G., Lacour S., Cami J., Haubois X., 2009, *A&A*, 504, 115
 Le Bertre T., Matthews L. D., Gérard E., Libert Y., 2012, *MNRAS*, 422, 3433
 Lim J., Carilli C. L., White S. M., Beasley A. J., Marson R. G., 1998, *Nat.*, 392, 575
 Lobel A., Dupree A. K., 2001, *ApJ*, 558, 815
 Morris R. a. H., 2001, PhD thesis, University of Wales, Cardiff
 Newell R. T., Hjellming R. M., 1982, *ApJ*, 263, L85
 Noriega-Crespo A., van Buren D., Cao Y., Dgani R., 1997, *AJ*, 114, 837
 O’Gorman E., Harper G. M., Brown J. M., Brown A., Redfield S., Richter M. J., Requena-Torres M. A., 2012, *AJ*, 144, 36
 Ohnaka, K. et al. 2011, *A&A*, 529, A163
 Percy J. R., Desjardins A., Yu L., Landis H. J., 1996, *PASP*, 108, 139
 Perrin G., Ridgway S. T., Coudé du Foresto V., Mennesson B., Traub W. A., Lacasse M. G., 2004, *A&A*, 418, 675
 Skinner C. J., Dougherty S. M., Meixner M., Bode M. F., Davis R. J., Drake S. A., Arens J. F., Jernigan J. G., 1997, *MNRAS*, 288, 295
 Tatebe K., Chandler A. A., Wishnow E. H., Hale D. D. S., Townes C. H., 2007, *ApJL*, 670, L21
 Thirumalai A., Heyl J. S., 2012, *MNRAS*, 422, 1272
 Tuthill P. G., Haniff C. A., Baldwin J. E., 1997, *MNRAS*, 285, 529
 Uitenbroek H., Dupree A. K., Gilliland R. L., 1998, *AJ*, 116, 2501
 Verhoelst, T. et al. 2006, *A&A*, 447, 311
 Weymann R., 1962, *ApJ*, 136, 844
 Wittkowski, M. et al. 2011, *A&A*, 532, L7

APPENDIX A: DATA PROCESSING SUMMARY**A1 Calibration**

This is a summary of the steps for data calibration. AIPS (Greisen 1994) was used for data processing as the required capabilities are not yet fully implemented in CASA. Data were stored in multi-source format, the time-dependent solution tables being interpolated into calibration tables using CLCAL. Separate solutions were derived for each spectral window and hand of circular polarization.

(i) Load data (FITLD), ensure that they are in time-baseline order (MSSORT) and inspect/edit. Editing (SPFLG, UVFLG and IBLED) was performed at a number of stages as required.

(ii) Derive delay and rate corrections per scan for calibration sources 0551+0829 and OQ208 (FRING).

(iii) Derive time-dependent phase, and then amplitude and phase solutions for calibration sources (CALIB).

(iv) Use the solutions for the three most similar antennas (Darnhall, Pickmere, Knockin) for a selected time interval, to establish the flux density of 0551+0829 by comparison with OQ208 (GETJY), refining the solutions by requiring a straight-line spectral index (SOUSPC).

Centre freq. (GHz)	5.4954	5.6874	5.8154	5.9434
OQ208 (Jy)	2.48	2.49	2.50	2.51
0551+0829 (Jy)	0.183	0.190	0.196	0.203

The flux density of OQ208 was derived from 3C286 (R. Beswick, private communication).

(v) Derive channel-by-channel amplitude and phase bandpass solutions for OQ208, averaging each half-hour scan (BPASS).

(vi) Apply the bandpass solutions using SPLAT and repeat steps (ii), (iii) and (v), using the established flux density of 0551+0829 as its model.

(vii) Split out Betelgeuse, applying all calibration.

(viii) Make a preliminary, naturally-weighted image (IMAGR). The star was clearly resolved, showing a bright central ridge and a halo a few hundred mas in size, strongest to the SW. AIPS fitted beam size of (0.195×0.074) arcsec, PA 143°. The major axis is more than double the true resolution (even at declination 7°), because the great sensitivity of the Lovell compared to the other telescopes creates a bias towards shorter baselines. All imaging used careful boxing and a small number of iterations (50–100).

(ix) Use the clean components as a model for phase-only self-calibration with a 7-min (per-scan) solution interval. These were applied and a new image of Betelgeuse was made. We also plotted the visibility amplitudes and noticed some residual, slowly-changing amplitude errors (lower amplitudes on shorter baselines, differences between hands of polarization). We carried out a final amplitude self-calibration with a 1 hr solution interval, which did not affect the source structure but improved the signal to noise ratio.

A2 Imaging

All images were made in total intensity, combining all spectral windows using a spectral index of 1.32 (using a flat spectral index made a very small difference, much less than the 10% total flux scale uncertainty). There is a trade-off between sensitivity to extended structure and resolution, in interferometry data. We chose two weighting schemes, based on the inherently different sensitivities of the e-MERLIN telescopes and on empirically established values to optimise either sensitivity or resolution without increasing the noise more than 10%. The Defford telescope is least sensitive and was given a weight of 0.1. The 75-m Lovell telescope (provid-

ing many short baselines) and the 32-m Cambridge telescope (providing the longest baselines) are the most sensitive at 5–6 GHz. We maximised sensitivity to extended structure by giving Lovell and Cambridge data weights of 10 and 2.4, respectively. We maximised resolution by giving both the Lovell and Cambridge data a weight of 4. All other (25-m) telescopes were given a weight of 1. The weighting was further modified in the AIPS task IMAGR by applying suitable interpolation into the missing spacings; a uvtaper of 3500 kλ with natural weighting for optimum sensitivity and partial uniform weighting ROBUST 0.75 for optimum resolution.

A3 Astrometry and photometry

We observed Betelgeuse at a pointing position of J2000 05:55:10.33 +07:24:25.6. The phase reference ICRF2 position of 05:51:11.2293 +08:29:11.221 is accurate to < 0.001 arcsec and it is only 1.5° from Betelgeuse. Inspection of the OQ208 raw phase corrections suggests this introduces an uncertainty of one turn of phase in 30 min of time on the longest baselines, corresponding to one beam in 7.5° of arc or 0.016 arcsec in 1.5°; the uncertainties in telescope positions introduce negligible errors. We measured the position of Betelgeuse for astrometric purposes by fitting a 2D Gaussian component to the naturally-weighted image before self-calibration.

The flux density scale is derived from 3C286; we do not yet have a full model of this source at e-MERLIN resolution and sensitivity so we conservatively estimate a 10% flux scale uncertainty. 0551+0829 has a spectral index of 1.3. We note that MERLIN observations in 1995 found a flux density of 0.128 Jy for 0551+0829 at 4.994 GHz, 20% lower than the flux density extrapolated from current observations. This is within the plausible variability of a compact QSO in 17 yr.